Astronomy & Astrophysics

Physical properties of trans-Neptunian object (143707) 2003 UY$_{117}$ derived from stellar occultation and photometric observations

M. Kretlow[1,*], J. L. Ortiz[1], J. Desmars[2,3], N. Morales[1], F. L. Rommel[10,5,7], P. Santos-Sanz[1], M. Vara-Lubiano[1], E. Fernández-Valenzuela[7,1], A. Alvarez-Candal[1,22], R. Duffard[1], F. Braga-Ribas[4,5], B. Sicardy[3], A. Castro-Tirado[1], E. J. Fernández-García[1], M. Sánchez[15], A. Sota[1], M. Assafin[9,5], G. Benedetti-Rossi[14,5,6], R. Boufleur[6], J. I. B. Camargo[13,5], S. Cikota[19], A. Gomes-Junior[8,5], J. M. Gómez-Limón[1], Y. Kilic[1,26], J. Lecacheux[6], R. Leiva[1], J. Marques-Oliveira[6], R. Morales[1], B. Morgado[9], J. L. Rizos[1], F. Roques[6], D. Souami[6,11,12], R. Vieira-Martins[13,5,9], M. R. Alarcon[21], R. Boninsegna[25], O. Çakır[29,30], F. Casarramona[23], J. J. Castellani[24], I. de la Cueva[16], S. Fişek[27,28], A. Guijarro[19], T. Haymes[24], E. Jehin[20], S. Kidd[24], J. Licandro[21], J. L. Maestre[17], F. Murgas[21], E. Pallé[21], M. Popescu[18], A. Pratt[24], M. Serra-Ricart[21], and J. C. Talbot[24]

(Affiliations can be found after the references)

ABSTRACT

Context. Trans-Neptunian objects (TNOs) are considered to be among the most primitive objects in our Solar System. Knowledge of their primary physical properties is essential for understanding their origin and the evolution of the outer Solar System. In this context, stellar occultations are a powerful and sensitive technique for studying these distant and faint objects.

Aims. We aim to obtain the size, shape, absolute magnitude, and geometric albedo for TNO (143707) 2003 UY$_{117}$.

Methods. We predicted a stellar occultation by this TNO for 2020 October 23 UT and ran a specific campaign to investigate this event. We derived the projected profile shape and size from the occultation observations by means of an elliptical fit to the occultation chords. We also performed photometric observations of (143707) 2003 UY$_{117}$ to obtain the absolute magnitude and the rotational period from the observed rotational light curve. Finally, we combined these results to derive the three-dimensional shape, volume-equivalent diameter, and geometric albedo for this TNO.

Results. From the stellar occultation, we obtained a projected ellipse with axes of $(282 \pm 18) \times (184 \pm 32)$ km. The area-equivalent diameter for this ellipse is $D_{\mathrm{eq,A}} = 228 \pm 21$ km. From our photometric R band observations, we derived an absolute magnitude of $H_V = 5.97 \pm 0.07$ mag using $V - R = 0.46 \pm 0.07$ mag, which was derived from a V band subset of these data. The rotational light curve has a peak-to-valley amplitude of $\Delta m = 0.36 \pm 0.13$ mag. We find the most likely rotation period to be $P = 12.376 \pm 0.0033$ hours. By combining the occultation with the rotational light curve results and assuming a triaxial ellipsoid, we derived axes of $a \times b \times c = (332 \pm 24)$ km $\times (216 \pm 24)$ km $\times (180_{-24}^{+28})$ km for this ellipsoid, and therefore a volume-equivalent diameter of $D_{\mathrm{eq,V}} = 235 \pm 25$ km. Finally, the values for the absolute magnitude and for the area-equivalent diameter yield a geometric albedo of $p_V = 0.139 \pm 0.027$.

Key words. methods: observational – techniques: photometric – astrometry – occultations – Kuiper belt objects: individual: (143707) 2003 UY$_{117}$

1. Introduction

Trans-Neptunian objects (TNOs), along with the objects coming from the Oort cloud, are considered to be the most primordial bodies in our Solar System. The study of their physical and dynamical properties helps us learn about their origin and evolution, which in turn provides crucial information about the origin and history of the early Solar System (Nesvorný & Morbidelli 2012). Currently, the Minor Planet Center (MPC) has counted about 5315 TNOs[1]. This includes the population of Centaurs, which are objects believed to be in a transition stage between TNOs and Jupiter-family comets (e.g., Horner et al. 2004; Sarid et al. 2019).

Because TNOs are located in the outer region of the Solar System, they are difficult to study. These objects typically exhibit low brightness, and with an average surface temperature of approximately $30-40$ K, their thermal emission peak occurs in the far-infrared spectrum, a range obstructed by Earth's atmosphere. To derive radiometric sizes, it is necessary to observe them with space telescopes, as was done for more than 120 TNOs and Centaurs within the ESA *Herschel* mission "TNOs are Cool" open-time key program (e.g., Müller et al. 2009; Lellouch et al. 2013; Farkas-Takács et al. 2020, and references therein). The *Herschel* mission was completed in 2013.

An alternative to the radiometric technique for deriving sizes and albedos is the use of stellar occultations. The observation of stellar occultations by small bodies (asteroids, comets, Centaurs, TNOs, and planetary moons) of the Solar System is an instrumental relatively simple, but powerful, technique for: directly measuring the size and shapes of these objects with (sub)kilometer accuracy, probing the environment around them with the possibility of revealing a binary nature (Leiva et al. 2020); discovering moons (e.g., Gault et al. 2022) and rings (Braga-Ribas et al. 2014; Ortiz et al. 2015, 2017); and detecting, measuring, or constraining an atmosphere down to the nanobar pressure level (e.g., Hubbard et al. 1988; Sicardy et al. 2003;

---

[1] Data retrieved from the MPC on 2024 January 22.

Oliveira et al. 2022). In addition, the occultation observation provides an astrometric measurement of the occulting object with (sub) milliarcsecond accuracy within the *Gaia* reference system (Rommel et al. 2020; Ferreira et al. 2022; Kaminski et al. 2023), which can be used to improve the orbit and therefore also predictions of future occultation events. In contrast to occultations by asteroids, predicting and successfully observing stellar occultations by TNOs can be very challenging, mainly due to the very small angular sizes of the TNOs together with the relatively large ephemeris uncertainties.

Trans-Neptunian object (143707) 2003 UY_{117} was discovered by the 0.9 m Spacewatch telescope at Steward Observatory (Kitt Peak, Arizona) on 2003 October 23 (MPEC 2003-V03), shortly before its perihelion in the year 2004. Prediscovery observations date back to the year 2001 (MPEC 2003-Y50). This TNO travels around the Sun in a highly eccentric orbit ($e \sim 0.4$), with a perihelion distance of $q \sim 32$ au and an aphelion distance of $Q \sim 78$ au. The MPC classifies 2003 UY_{117} as a scattered disc object (SDO), but not very much is known about its physical properties. Sheppard (2012) obtained an absolute magnitude of $H_R = 5.35 \pm 0.03$ mag and a color index of $V - R = 0.56 \pm 0.01$ mag, and therefore $H_V = 5.91 \pm 0.04$ mag. Alvarez-Candal et al. (2019) reported $H_V = 6.13 \pm 0.04$ mag, $H_R = 5.60 \pm 0.04$ mag, and $V - R = 0.53 \pm 0.06$ mag.

The geometric albedo, p_V, and diameter, D, of a small body are related via (e.g., Russell 1916; Harris 1998)

$$D = \frac{D_0}{\sqrt{p_V}} 10^{-H_V/5}, \qquad (1)$$

where H_V is the absolute magnitude of the object, $D_0 = 2$ au $\cdot$ $10^{V_\odot/5}$, and $V_\odot$ is the apparent visual magnitude of the Sun. Values for the apparent magnitude of the Sun are $V_\odot = -26.76$ mag (Willmer 2018) and $V_\odot = -26.74$ mag (Rieke et al. 2008), resulting in $D_0 = 1330.2$ km and $D_0 = 1342.6$ km, respectively. An earlier (commonly known and often used) value is $D_0 = 1329$ km. Applying Eq. (1), with $D_0 = 1330.2$ km and assuming a geometric albedo, p_V, of either 6.9% or 17% for 2003 UY_{117} as proposed by Santos-Sanz et al. (2012) for SDOs, yields effective diameters of about 333 km and 212 km, respectively. Farkas-Takács et al. (2020) derived an effective diameter of $D = 196^{+114}_{-54}$ km for 2003 UY_{117} from *Herschel* (PACS[2]) thermal observations (using an absolute magnitude of $H_V = 5.91$ mag in their work).

In this paper, we report the observation of a stellar occultation by 2003 UY_{117} and the results we obtained from it (Sect. 2). We also obtained photometric observations in order to derive the absolute magnitude and the rotation period of 2003 UY_{117} (Sect. 3). Finally, we combined these results in order to constrain the three-dimensional size of the body and to derive the geometric albedo (Sect. 4).

2. 2020 October 23 occultation

2.1. Prediction

Within the Lucky Star collaboration[3], we predicted a stellar occultation of a $G = 14.5$ mag star for 2020 October 23 using the *Gaia* DR2 star catalog and the NIMA[4] ephemeris (Desmars et al. 2015). Table 1 summarizes the occultation parameter and the details of the occulted star. The prediction details in Table 1 were taken from the nominal NIMA (version 3) prediction[5]. The

Table 1. 2020 October 23 occultation circumstances and target star data.

Occultation parameter (NIMAv3 prediction)	
Date and time of closest approach (t_0)	2020-10-23 22:18:08 UT ± 78 s
Geocentric shadow velocity	21.80 km/s
Magnitude drop	6.6 mag
Maximum duration	13.1 s
Apparent diameter of 2003 UY_{117}	12 mas
Occulted star data (from *Gaia* DR2)	
Gaia DR2 source ID	62553763421986304
Proper motion (mas/yr)	$\mu_{\alpha}* = +13.5 \pm 0.1$ $\mu_{\delta} = +0.5 \pm 0.0$
Position (ICRS, cat. epoch)	$\alpha = 03\ 23\ 26.2108$ $\delta = +22\ 47\ 19.192$
Position (ICRS, occ. epoch)	$\alpha = 03\ 23\ 26.2160$ $\delta = +22\ 47\ 19.195$
Position error (occ. epoch)	$\sigma_{\alpha*} = 0.3$ mas $\sigma_{\delta} = 0.3$ mas
G, RP, BP magnitudes	14.54, 13.80, 15.17
V, R, B magnitudes (from NOMAD)	14.54, 14.27, 15.25
J, H, K magnitudes (from NOMAD)	12.84, 12.41, 12.22
Occulted star data (from *Gaia* DR3)	
Proper motion (mas/yr)	$\mu_{\alpha}* = +13.320 \pm 0.049$ $\mu_{\delta} = +0.388 \pm 0.029$
Position (ICRS, cat. epoch)	$\alpha = 03\ 23\ 26.2113$ $\delta = +22\ 47\ 19.192$
Position (ICRS, occ. epoch)	$\alpha = 03\ 23\ 26.2155$ $\delta = +22\ 47\ 19.194$
Position error (occ. epoch)	$\sigma_{\alpha*} = 0.24$ mas $\sigma_{\delta} = 0.14$ mas
RUWE	1.05
Duplicated source	false

Notes. The maximum occultation duration (central line) and the apparent diameter of the TNO are given for an assumed size of $D = 285$ km. The V, R, B, J, H, and K magnitudes of the target star were taken from the NOMAD catalog (Zacharias et al. 2004). The renormalized unit weight error (RUWE) is a measure of the reliability of a single-star model derived from observations. A value close to 1 is typically expected. Values exceeding 1.4 could indicate that the source is not a single star or that there are problems with the astrometric solution. The duplicated source flag also indicates that multiple sources were obtained during data processing[6].

target star data from *Gaia* DR3 are also given for comparison. About a week before the occultation date, we updated and refined the prediction using high-precision astrometry ($\sigma \sim 15$ mas) that we obtained with the 2 m Liverpool Telescope (LT) at Roque de Los Muchachos Observatory (ORM) on the island of La Palma, Spain. The update shifted the ground track farther to the north into a region with even better observability potential, especially for the European region, with a dense network of telescopes and observers (Fig. 1). We then organized an observation campaign to detect the occultation from as many sites as possible. We used the Occultation Portal (Kilic et al. 2022)[7] for observation reporting and data storage.

2.2. Observations

The weather conditions were unfavorable during the event for large parts of the occultation path. However, we obtained four

---

[2] Photodetector Array Camera and Spectrometer.
[3] https://lesia.obspm.fr/lucky-star/
[4] Numerical Integration of the Motion of an Asteroid.
[5] https://lesia.obspm.fr/lucky-star/occ.php?p=41240

[6] https://gea.esac.esa.int/archive/documentation/ GEDR3/Gaia_archive/chap_datamodel/sec_dm_main_tables/ ssec_dm_gaia_source.html
[7] https://occultation.tug.tubitak.gov.tr/

Table 2. Ingress and egress times (UT) obtained for the 2020 October 23 occultation.

#	Site name	Ingress (UT)	I.err	Egress (UT)	E.err	Duration	Chord length
1	Arenosillo	22:21:49.83	0.69 s	22:22:00.44	0.54 s	10.61 s	231 km
2	Granada	22:21:42.36	0.14 s	22:21:50.48	0.08 s	8.12 s	177 km
3	OSN90	22:21:41.12	1.25 s	22:21:48.45	0.23 s	7.34 s	160 km
4	OSN150	22:21:42.18	1.03 s	22:21:49.13	0.26 s	6.94 s	151 km

Notes. Also given are the 1σ errors of the ingress and egress times, the occultation duration in seconds, and the corresponding chord length in km.
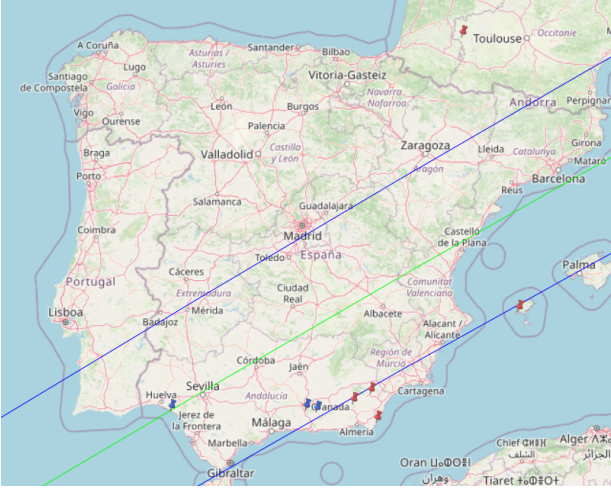
Fig. 1. Map of the ground track of our latest prediction update, based on astrometry obtained at the 2 m LT on La Palma. A spherical diameter of $D = 285$ km was used for 2003 UY$_{117}$ for the predicted shadow path width (blue lines) plotted in this figure. The map also displays the sites where the occultation was observed, with blue markers indicating a positive detection and red ones indicating a negative detection (i.e., a "miss"). Negative observations reported from Belgium and England, which were located within the uncertainty of the original nominal prediction, are outside this map. Map credit: OpenStreetMap.

positive detections from three different locations in Spain. Additionally, we recorded three very close misses to the south of the body from Spain and ten misses from another nine observing sites (see Fig. 1 and Table A.1 for observation details). We utilized synthetic aperture photometry to obtain the occultation light curves from the observations. The four positive detections are shown in Fig. 2.

The star's apparent diameter was calculated to be 0.0178 mas (V-mag) and 0.0172 mas (B-mag) using the formulae published by Kervella et al. (2004). This translates to a distance of 0.4 km at the projected distance of 2003 UY$_{117}$ ($\Delta = 33.47$ au), or 0.02 s for the shadow velocity of 21.80 km/s. The Fresnel scale $R_F = \sqrt{\lambda \cdot \Delta/2}$ is 1.32 km, or 0.06 s for a wavelength of $\lambda = 700$ nm. As all positive detections were recorded with exposure times ≥ 2 s, any effects due to diffraction or the apparent stellar diameter are negligible.

The ingress (disappearance) and egress (reappearance) times were extracted from the fitted occultation light curves and were translated into chords on the sky plane. To model the light curves and to fit the profile, we utilized the SORA[8] Python package (Gomes-Júnior et al. 2022), which also facilitates the extraction of ingress and egress times. The extracted times are listed in Table 2.
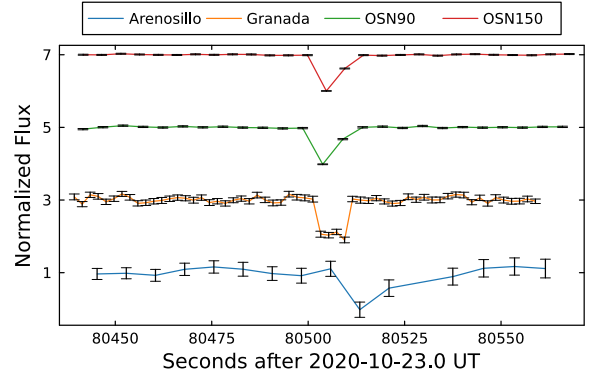

Fig. 2. Occultation light curves. The light curves (flux vs. time) are normalized and shifted from each other on the y-axis by an offset value of 2 for clarity. The site, telescope, and instrument details are given in Table A.1.

2.3. Profile fit

Assuming a spheroidal or an ellipsoidal object, the projected cross section on the sky plane is an ellipse. Therefore, we fit an ellipse to the extremities of the chords (derived from the ingress and egress times as described in Sect. 2.2), taking into account the near misses of the occultation as an additional constraint (Fig. 3). The five solve-for parameters were: the center of the ellipse (f, g) with respect to the center of the fundamental plane defined by the geocentric star and TNO position for the event time; the semimajor axis, a'; the oblateness, $\epsilon' = (a' - b')/a'$; and the position angle of the ellipse, φ'[9]. The prime ($'$) indicates that these parameters belong to the projected ("apparent") profile ellipse of the object and distinguishes them from the axes of a physical body (triaxial ellipsoid with semiaxes $a, b,$ and c). The parameters were estimated using the Levenberg-Marquardt optimization algorithm. The goodness of the fit was evaluated from the χ^2 per degree of freedom (pdf) value, defined as $\chi^2_{\mathrm{pdf}} = \chi^2/(N - M)$, where $N = 8$ is the number of data points and $M = 5$ is the number of adjustable parameters. Ideally, this value should be close to one. We obtain $\chi^2_{\mathrm{pdf}} = 0.43$ for our fit. The 1σ uncertainties in the retrieved parameters were obtained from a grid search in the parameter space, by varying one parameter from its nominal solution value while keeping the other parameters constant. Acceptable values were those that gave a χ^2 between χ^2_{min} and $\chi^2_{\mathrm{min}} + 1$. The results of our instantaneous best-fitting limb are summarized in Table 3.

3. Photometry

To interpret the occultation results with respect to the three-dimensional shape and size of the physical body, we carried out

---

8 Stellar Occultation Reduction and Analysis.

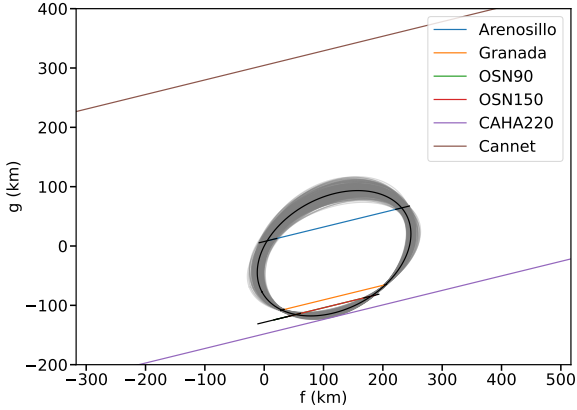9 The (clockwise positive) angle between the "g-positive" direction (i.e., north) and the semiminor axis, b'.

Fig. 3. Elliptical fit to the 2020 October 23 occultation observations (chords). This fit describes the limb of 2003 UY$_{117}$ for the moment of the occultation on the sky plane, defined by the (f, g) axes. As two chords were derived from the same site (OSN90 and OSN150; Sierra Nevada Observatory), they are not distinguishable in the plot. Also shown is the chord for the nearest site to the south (CAHA220: Calar Alto Observatory, 2.2 m telescope) and to the north (Cannet), both of which had a negative detection ("miss"). The gray shaded area is the 1σ uncertainty region of the derived ellipse.

Table 3. Elliptical occultation limb profile fit result.

Center coordinates (f,g)	$(119 \pm 7, -10 \pm 8)$ km
Semimajor axis a'	141 ± 9 km
Semiminor axis b'	94 ± 16 km
Position angle φ'	-31 ± 11 deg
Oblateness ϵ'	0.33 ± 0.11
Area-equiv. diameter $D_{\mathrm{eq,A}}$	228 ± 21 km
Best-fit χ^2_{pdf}	0.43

Notes. The fitted ellipse center (f,g) is with respect to the JPL#20 Horizons ephemeris.

photometric observations of 2003 UY$_{117}$ to determine its rotational light curve. We carried out observations with the 1.5 m telescope at Sierra Nevada Observatory (Spain) and with the 1.23 m telescope at Calar Alto Observatory (Spain) over six nights and with longer time coverage than the observations with the 2 m LT on La Palma (Sect. 2.1); the latter were done with the IO:O instrument and a Sloan r' filter, and were focused on astrometry with the aim of updating the occultation prediction. We also used sparse observations made at Calar Alto in 2019 by our group. Observations at the 1.5 m telescope were made with an Andor iKon-L CCD camera (model DZ936N-BEX2-DD)[10] without filters in order to increase the signal-to-noise ratio. At the 1.23 m telescope, we used the DLR-MKIII instrument[11] (also without filters), except for two nights when we took images with V and R filters to determine the $V - R$ color of the TNO. Image calibration and photometry were performed using the same algorithms and procedures as for the LT images (Sect. 2.1). The science images were calibrated in the usual manner, namely, bias and flat field image correction were applied to them.

3.1. Absolute magnitude

From the calibrated CCD images, we derived magnitudes in the R band using our algorithms that use the *Gaia* DR2 field stars

---
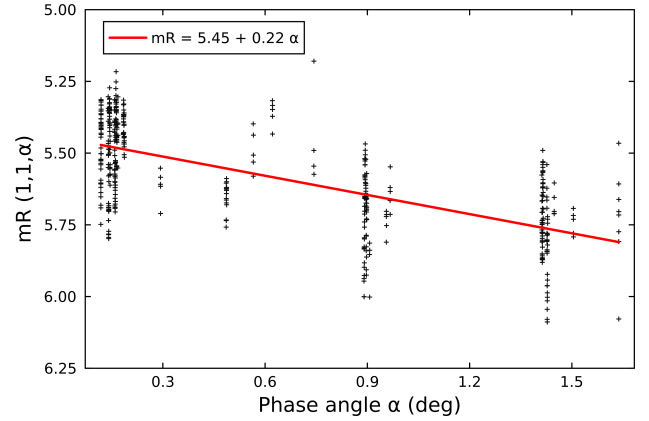
[10] https://www.osn.iaa.csic.es/en/page/ccdt150-and-ccdt90-cameras
[11] https://www.caha.es/es/telescope-1-23m-2/ccd-camera

Fig. 4. Reduced magnitude $m_R(1, 1, \alpha)$ vs. the phase angle, α. In total, 431 observations obtained with the 2 m LT, with the 1.5 m telescope at Sierra Nevada Observatory, and with the 1.23 m telescope at Calar Alto Observatory were used. The brightness variation cluster is due to the rotation of 2003 UY$_{117}$.

to determine photometric transformation equations, which take the color information into account (Morales et al. 2022). For the color of the TNO, we used a value of $V - R = 0.46 \pm 0.07$ mag, which was derived from two nights of observations with the Calar Alto 1.23 m telescope. From a linear regression of the reduced R magnitude (the apparent magnitude that the TNO would have at 1 au from the Sun and Earth) at several phase angles, α, we obtained the absolute magnitude, $H_R \equiv m_R(1, 1, 0)$, and the phase slope, β (Fig. 4). From the fitted trend line, we derived an absolute magnitude of $H_R = 5.45 \pm 0.01$ mag and a slope parameter of $\beta = 0.22 \pm 0.01$ mag/°. Our observations covered the phase angle range $\alpha = [0.118°, 1.638°]$. The scatter around the trend line indicates a significant rotational modulation.

3.2. Rotational light curve

After de-trending[12] the reduced and light-travel-time-corrected photometry, we performed a search for the rotation period of 2003 UY$_{117}$ using different period-finding techniques. In total, we had more than 400 observations from 2019 November 30 to 2021 February 15. We used the Lomb-Scargle (LS; Lomb 1976; Scargle 1982) algorithm to estimate the most likely rotation period from our data. The algorithm works in the frequency domain, and the most prominent light curve frequencies (in units of 1/day as the timescale of the data is days) are shown in the LS periodogram (Fig. 5). The normalized spectral power reveals a frequency of about 4/day (the exact value is $f = 3.878329$) as the dominant frequency. Given that a small (ellipsoidal) body typically executes two light curve periods in a single rotation period, the most likely rotation frequency is $f = 3.878329/2$ (day^{-1}), which corresponds to a rotation period of $P = 12.3765$ h.

To further constrain and verify the rotation period, we folded the data with a period in the range 4–30 h in 0.00001 day steps. For each period value, we fit a second-order Fourier series to the folded data and calculated the root mean square error (RMSE; Fig. 6). Additionally, we verified the phased plots for the most prominent periods that were derived in both approaches, and we also evaluated split-halves plots. The period with the smallest RMSE is $P = 12.3763$ h, which we chose as our best estimate for the rotation period of 2003 UY$_{117}$. The second prominent

---

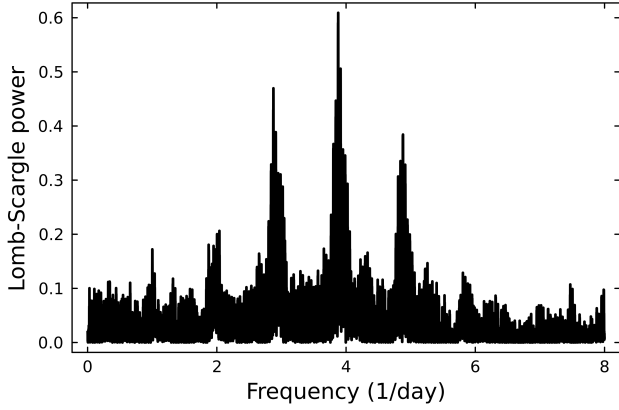[12] i.e., using the O-C residuals of the linear fit described in Sect. 3.1.

Fig. 5. LS periodogram. The rotational light curve frequency is given in 1/day. These values are light curve frequencies (periods); since a small body typically executes two light curve periods in a single rotation period, the best rotation period we obtain from the LS analysis is $P = 12.3765$ h.
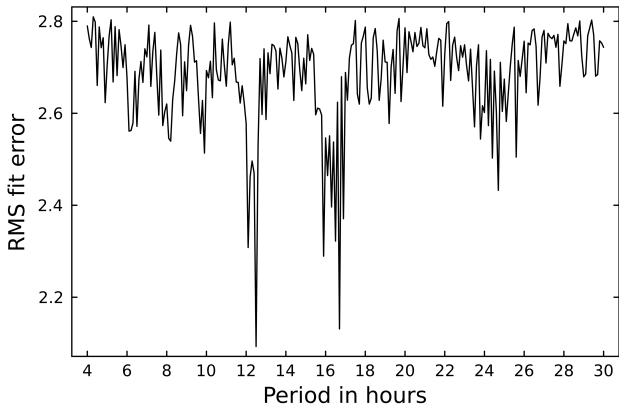

Fig. 6. Fourier fit periodogram. We scanned the period range 4−30 hours in 0.00001 h steps, folded the photometric data with the selected period, and fit a second-order Fourier series to the data. The best period we obtained, $P = 12.3763$ h, is the value for which the RMS of the residuals (data minus fit) reaches a minimum.

minimum at 16.692 h (Fig. 6) corresponds to 2.8756 cycles/day, which is a 24 h alias of the 1.9392 cycles/day frequency that corresponds to our preferred period of 12.376 h. The periodogram in cycles/day (Fig. 5) in addition to the periodogram in hours helps to identify 24 h aliases of the main peak, which are usually separated by ~1 cycle/day. From the results of the two approaches, we conclude that the rotation period is $P = 12.376 \pm 0.0033$ h[13]. From the best Fourier fit (Fig. 7), we derived a peak-to-valley amplitude of $\Delta m = 0.36 \pm 0.13$ mag.

4. Results

4.1. Size and shape

The instantaneous occultation ellipse limb fit to the projected profile of 2003 UY$_{117}$ (Fig. 3) yields $a' = 141 \pm 9$ km, $b' = 94 \pm 16$ km, and $\varphi' = -31° \pm 11°$ with a $\chi^2_{\text{pdf}} = 0.43$ value (Table 3). Given the large amplitude of the rotational light curve, we can expect that the intensity variations are due to shape effects, and this implies that 2003 UY$_{117}$ is not a spheroid. We assumed that a
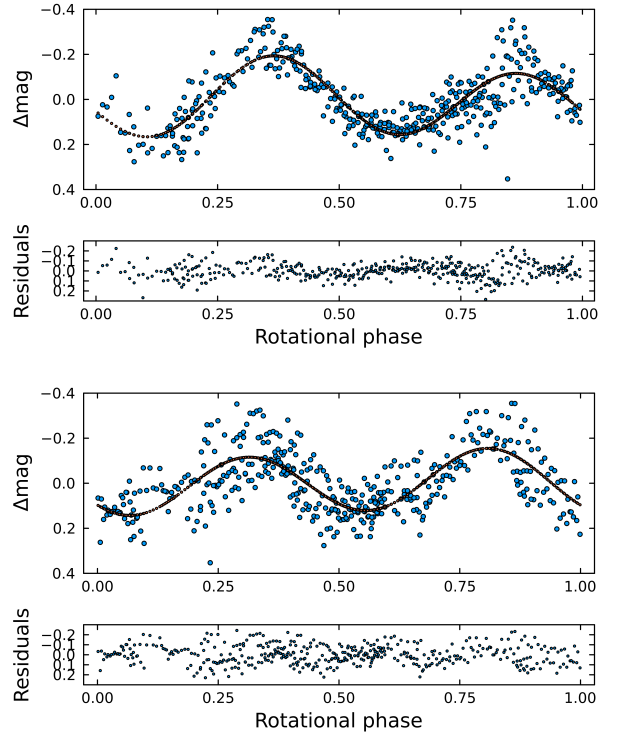
---

[13] The 1σ error was derived from the period value differences corresponding to χ^2_{min} and $\chi^2_{\text{min}} + 1$.

Fig. 7. Phased rotational light curve for 2003 UY$_{117}$ using all the photometric data folded with a period of $P = 12.376$ h (upper panel) and $P = 16.692$ h (lower panel). The $P = 12.376$ h is our preferred solution. This double-peaked light curve with an amplitude of 0.36 mag indicates a highly nonspherical body with a presumable triaxial shape. Phase 0.0 corresponds to the moment of mid-occultation for the observed occultation chords.

triaxial ellipsoid with semiaxes $a > b > c$ (spin-axis c) is a good approximation for the physical body. In the following, we deduce the possible shape and size of this ellipsoid from the occultation observation combined with our light curve results. Using the Maclaurin sequence equations (Chandrasekhar 1969), a hydrostatic equilibrium body rotating at ~12 h down to a density of $\rho \sim 0.2$ g/cm^3 would have taken on a Maclaurin spheroid shape, but 2003 UY$_{117}$ clearly does not have an (oblate) spheroid shape. Valid triaxial ellipsoids in hydrostatic equilibrium (Jacobi solutions) are possible only for densities ranging from 0.254 g/cm^3 to 0.333 g/cm^3 given the rotation period of 12.38 h. These densities are too low to be realistic for bodies in this size range.

The orthogonal projection of a triaxial ellipsoid (axes $a > b > c$, rotating around c) for a given spin state, expressed by the aspect angle, ψ (i.e., the angle between the rotation axis, c, and the line of sight) and the rotational phase, ϕ, is (e.g., Magnusson 1986)

$$A = b^2 c^2 \sin^2 \psi \sin^2 \phi + a^2 c^2 \sin^2 \psi \cos^2 \phi + a^2 b^2 \cos^2 \psi, \quad (2)$$

$$-B = a^2(\cos^2 \psi \sin^2 \phi + \cos^2 \phi) + b^2(\cos^2 \psi \cos^2 \phi + \sin^2 \phi)$$
$$+ c^2 \sin^2 \psi, \quad (3)$$

$$a' = \left(\frac{2A}{-B - (B^2 - 4A)^{1/2}} \right)^{1/2}, \quad (4)$$

$$b' = \left(\frac{2A}{-B + (B^2 - 4A)^{1/2}} \right)^{1/2}, \quad (5)$$

where (a', b') are the projected semiaxes that correspond to the apparent semiaxes of the projected cross section of an ellipsoidal

object during a stellar occultation. The rotational light curve amplitude for such an ellipsoid can be calculated as (e.g., Binzel et al. 1989, p. 426)

$$\Delta m = 2.5 \log\left(\frac{a}{b}\right) - 1.25 \log\left(\frac{a^2 \cos^2(\psi) + c^2 \sin^2(\psi)}{b^2 \cos^2(\psi) + c^2 \sin^2(\psi)}\right). \qquad (6)$$

By performing a grid search for the three body semiaxes, a, b, and c, and the polar aspect angle, ψ, using the rotational phase angle, ϕ, for the observed occultation time, we can find the best fit to the projected shape derived from the occultation while simultaneously fitting the rotational light curve amplitude (Δm). The rotational phase at the time of the observed 2020 October 23 occultation was ~0.63, measured from the absolute maximum of brightness (Fig. 7). The observed peak-to-valley amplitude is $\Delta m = 0.36 \pm 0.13$ mag. We defined the cost function to be minimized as $\chi^2 = (0.36 - \Delta m_c)^2/0.13^2 + (1.5 - a'/b')^2/0.35^2 + (141 - a')^2/9^2$, with the modeled light-curve amplitude, Δm_c, derived by Eq. (6), and the apparent semiaxes a', b' as obtained from Eqs. (4)–(5) for each triaxial ellipsoid "clone" (defined by a, b, c, and ψ; $\phi = 0.63 \cdot 2\pi$) created during the grid search. The scanned parameter space was $c = [60, 120]$ km, $b = [c, 160]$ km, and $a = [b, 200]$ km, with a grid spacing of 2 km. The aspect angle, ψ, was scanned between 0 and 90 degrees in 1° steps. From this search, we obtained a family of possible solutions of triaxial ellipsoids and aspect angles. The model that minimizes χ^2 has axes $a = 166 \pm 12$ km, $b = 108 \pm 12$ km, and $c = 90^{+14}_{-12}$ km, with an aspect angle of $\psi = 70^{+20}_{-12}$ deg. The diameter (of an equal-volume sphere) for this solution is $D_{eq} = 235 \pm 25$ km. The 1σ uncertainties in the retrieved parameters were obtained by varying one parameter from its nominal solution value with corresponding $\chi^2 = \chi^2_{min}$ up to $\chi^2 = \chi^2_{min} + 1$, while keeping the other parameters constant.

The spin axis orientation for this object is currently unknown. But if the pole orientation (α_p, δ_p) is known, the aspect angle can be computed as

$$\cos\psi = \sin\delta \sin\delta_p + \cos\delta \cos\delta_0 \cos(\alpha - \alpha_p), \qquad (7)$$

where α, δ are the coordinates of the object for the date of interest (e.g., the occultation date). By means of a grid search over the whole parameter space in 1° steps, we obtained a pole orientation of $(\alpha_p, \delta_p) = (337° \pm 10°, 62° \pm 5°)$.

4.2. Absolute magnitude and albedo

From our photometric observations, we obtained an absolute magnitude of $H_R = 5.45 \pm 0.01$ mag and a phase slope coefficient of $\beta = 0.22 \pm 0.01$ mag/° for 2003 UY$_{117}$ (Fig. 4). Taking into account the brightness contribution due to the rotational phase at the occultation time (about 0.06 mag), and using a color value $V - R = 0.46 \pm 0.07$ mag, which we got from our observations as well, this yields $H_R = 5.51 \pm 0.01$ mag and $H_V = 5.97 \pm 0.07$ mag. Our $V - R$ value is slightly smaller than the $V - R$ value of 0.56 ± 0.01 mag reported by Sheppard (2012) and the $V - R = 0.59 \pm 0.01$ mag reported by Tegler et al. (2016). Sheppard and Tegler derived absolute magnitudes of $H_R = 5.35 \pm 0.03$ mag and $H_V = 5.91$ mag, respectively. Taking into account the large light curve amplitude (which was not considered in the estimates derived by these authors), their values are compatible with ours within the error bars. Our result also agrees with the values of $H_R = 5.60 \pm 0.04$ mag, $H_V = 6.13 \pm 0.04$ mag, and $V - R = 0.53 \pm 0.06$ mag obtained by Alvarez-Candal et al. (2019), where a half rotational light curve amplitude value of $\Delta m/2 = 0.06$ mag

was also considered in the parameter estimation. By applying Eq. (1) with the values $D_0 = 1330.2$ km, $D_{eq,A} = 228 \pm 21$ km as area-equivalent diameter, and $H_V = 5.97 \pm 0.07$ mag, we get a geometric albedo of $p_V = 0.139 \pm 0.027$ for 2003 UY$_{117}$.

4.3. Astrometry

The ellipse center coordinates given in Table 3, $(119 \pm 7, -10 \pm 8)$ km, are two of the five solve-for parameters of the ellipse fit and represent the offset (O-C) between the observed and the predicted position (defined by the object ephemeris and the star position). This information was used to calculate the object position. We derived an astrometric place (ICRS[14]) for 2003 UY$_{117}$ at 22:19:21.8 UT on 2020 October 23 with equatorial coordinates

α (hms) = 03 23 26.21404 $\pm$ 0.3 mas,
δ (dms) = +22 47 19.3184 $\pm$ 0.4 mas.

This high-precision astrometry will be used in our orbit determination of the TNO and will also improve the accuracy of future occultation predictions.

5. Conclusions

- A stellar occultation by TNO (143707) 2003 UY$_{117}$ has been predicted and successfully observed for the first time. From four occultation chords observed at three different sites, we derived an instantaneous projected elliptical size of the object with dimensions $(282 \pm 18) \times (184 \pm 32)$ km. The area-equivalent diameter is $D_{eq,A} = 228 \pm 21$ km.
- We also obtained the absolute magnitude, phase slope, $V - R$ color, and rotation period for this TNO from our photometric observation campaign. Our preferred rotation period, P, is 12.376 ± 0.0033 hours. The light curve is double-peaked with a peak-to-valley amplitude of $\Delta m = 0.36 \pm 0.13$ mag. We obtained an absolute magnitude of $H_R = 5.51 \pm 0.01$ mag and $H_V = 5.97 \pm 0.07$ mag using a $V - R = 0.46 \pm 0.07$ mag value, which was also derived from our observations. From the area-equivalent diameter of $D_{eq,A} = 228 \pm 21$ km and the absolute magnitude, H_V, given above, we derived a geometric albedo of $p_V = 0.139 \pm 0.027$.
- By combining the occultation with the rotation light curve results, we derived tight constraints on the three-dimensional size and shape of 2003 UY$_{117}$. Our best solution is $2a = 332 \pm 24$ km, $2b = 216 \pm 24$ km, and $2c = 180^{+28}_{-24}$ km for a triaxial body, which yields an equivalent spherical diameter of $D_{eq} = 235 \pm 25$ km. This value is slightly larger than the radiometric result $D_{eq} = 196^{+114}_{-54}$ km (Farkas-Takács et al. 2020), but well within the error margins. The aspect angle we derived for the occultation epoch is $\psi = 70^{+20}_{-12}$ deg. A pole solution that is compatible with the findings above is $(\alpha_p, \delta_p) = (337° \pm 10°, 62° \pm 5°)$.
- We derived an occultation-based astrometric position (ICRS) for 2003 UY$_{117}$.

---

[14] International Celestial Reference System.

References

Alvarez-Candal, A., Ayala-Loera, C., Gil-Hutton, R., et al. 2019, MNRAS, 488, 3035

Binzel, R. P., Gehrels, T., & Matthews, M. S. 1989, Asteroids II (Tucson: University of Arizona Press)

Braga-Ribas, F., Sicardy, B., Ortiz, J. L., et al. 2014, Nature, 508, 72

Chandrasekhar, S. 1969, Ellipsoidal Figures of Equilibrium (New Haven and London: Yale University Press)

Desmars, J., Camargo, J. I. B., Braga-Ribas, F., et al. 2015, A&A, 584, A96

Farkas-Takács, A., Kiss, Cs., Vilenius, E., et al. 2020, A&A, 638, A23

Ferreira, J. F., Tanga, P., Spoto, F., Machado, P., & Herald, D. 2022, A&A, 658, A73

Gault, D., Nosworthy, P., Nolthenius, R., Bender, K., & Herald, D. 2022, Minor Planet Bull., 49, 3

Gomes-Júnior, A. R., Morgado, B. E., Benedetti-Rossi, G., et al. 2022, MNRAS, 511, 1167

Harris, A. W. 1998, Icarus, 131, 291

Horner, J., Evans, N. W., & Bailey, M. E. 2004, MNRAS, 354, 798

Hubbard, W. B., Hunten, D. M., Dieters, S. W., Hill, K. M., & Watson, R. D. 1988, Nature, 336, 452

Kaminski, K., Weber, C., Marciniak, A., Zolnowski, M., & Gedek, M. 2023, PASP, 135, 025001

Kervella, P., Thévenin, F., Di Folco, E., & Ségransan, D. 2004, A&A, 426, 297

Kilic, Y., Braga-Ribas, F., Kaplan, M., et al. 2022, MNRAS, 515, 1346

Leiva, R., Buie, M. W., Keller, J. M., et al. 2020, Planet. Sci. J., 1, 48

Lellouch, E., Santos-Sanz, P., Lacerda, P., et al. 2013, A&A, 557, A60

Lomb, N. R. 1976, Astrophys. Space Sci., 39, 447

Magnusson, P. 1986, Icarus, 68, 1

Morales, N., Ortiz, J. L., Morales, R., et al. 2022, Europlanet Science Congress 2022, EPSC2022-664

Müller, T. G., Lellouch, E., Böhnhardt, H., et al. 2009, Earth Moon Planet, 105, 209

Nesvorný, D., & Morbidelli, A. 2012, AJ, 144, 117

Oliveira, J. M., Sicardy, B., Gomes-Júnior, A. R., et al. 2022, A&A, 659, A136

Ortiz, J. L., Duffard, R., Pinilla-Alonso, N., et al. 2015, A&A, 576, A18

Ortiz, J. L., Santos-Sanz, P., Sicardy, B., et al. 2017, Nature, 550, 219

Rieke, G. H., Blaylock, M., Decin, L., et al. 2008, AJ, 135, 2245

Rommel, F. L., Braga-Ribas, F., Desmars, J., et al. 2020, A&A, 644, A40

Russell, H. N. 1916, ApJ, 43, 173

Santos-Sanz, P., Lellouch, E., Fornasier, S., et al. 2012, A&A, 541, A92

Sarid, G., Volk, K., Steckloff, J. K., et al. 2019, ApJ, 883, L25

Scargle, J. D. 1982, ApJ, 263, 835

Sheppard, S. S. 2012, AJ, 144, 169

Sicardy, B., Widemann, T., Lellouch, E., et al. 2003, Nature, 424, 168

Tegler, S. C., Romanishin, W., Consolmagno, G. J., & J., S. 2016, AJ, 152, 210

Willmer, C. N. A. 2018, ApJS, 236, 47

Zacharias, N., Monet, D. G., Levine, S. E., et al. 2004, Am. Astron. Soc. Meet. Abstr., 205, 48.15

[1] Instituto de Astrofísica de Andalucía, IAA-CSIC, Glorieta de la Astronomía s/n, 18008 Granada, Spain

[2] Institut Polytechnique des Sciences Avancées IPSA, 94200 Ivrysur-Seine, France

[3] IMCCE, Observatoire de Paris, PSL Research University, CNRS, Sorbonne Université, Univ. Lille, 75014 Paris, France

[4] Federal University of Technology-Paraná (UTFPR/PPGFA), Curitiba, PR, Brazil

[5] Laboratório Interinstitucional de e-Astronomia - LIneA - and INCT do e-Universo, Av. Pastor Martin Luther King Jr, 126 - Del Castilho, Nova América Offices, Torre 3000 / sala 817, Rio de Janeiro, RJ 20765-000, Brazil

[6] LESIA, Observatoire de Paris, Université PSL, CNRS, Sorbonne Université, 5 place Jules Janssen, 92190 Meudon, France

[7] Florida Space Institute, University of Central Florida, Orlando, FL 32826-0650, USA

[8] Federal University of Uberlândia (UFU), Physics Institute, Av. João Naves de Ávila 2121, Uberlândia, MG 38408-100, Brazil

[9] Universidade do Rio de Janeiro - Observatório do Valongo, Ladeira do Pedro Antonio 43, Rio de Janeiro, RJ 20.080-090, Brazil

[10] Federal University of Technology - Paraná (PPGFA/UTFPR-Curitiba), Av. Sete de Setembro, 3165 Curitiba, PR, Brazil

[11] Departments of Astronomy and of Earth and Planetary Science, 501 Campbell Hall, University of California, Berkeley, CA 94720, USA

[12] naXys, Department of Mathematics, University of Namur, Rue de Bruxelles 61, 5000 Namur, Belgium

[13] Observatório Nacional/MCTI, Rua Gal. José Cristino 77, Rio de Janeiro RJ 20921-400, Brazil

[14] UNESP-São Paulo State University, Grupo de Dinâmica Orbital e Planetologia, CEP 12516-410 Guaratinguetá, SP, Brazil

[15] Sociedad Astronómica Granadina , Apartado de Correos 195, 18080 Granada, Spain

[16] Agrupación Astronómica de Eivissa, C. Lucio Oculacio s/n, 07800 Ibiza, Spain

[17] Observatorio Astronómico de Albox, Apt. 63, 04800 Albox, Almeria, Spain

[18] Astronomical Institute of the Romanian Academy, 5 Cuțitul de Argint, 040557 Bucharest, Romania

[19] Centro Astronómico Hispano en Andalucía, Observatorio de Calar Alto, Sierra de los Filabres, 04550 Gérgal, Almeria, Spain

[20] University of Liège, 4000 Liège, Belgium

[21] Instituto de Astrofísica de Canarias (IAC), C/Vía Láctea s/n, 38205 La Laguna, Tenerife, Spain

[22] Instituto de Física Aplicada a las Ciencias y las Tecnologías,U niversidad de Alicante, Alicante, San Vicente del Rapeig, Spain

[23] Agrupación Astronómica de Sabadell, Prat de la Riba sn, 08206 Sabadell, Spain

[24] International Occultation Timing Association/European Section, Am Brombeerhag 13, 30459 Hannover, Germany

[25] Rue de Mariembourg 45, 5670 Dourbes, Belgium

[26] TÜBITAK National Observatory, Akdeniz University Campus, 07058 Antalya, Turkey

[27] Department of Astronomy and Space Sciences, Faculty of Science, Istanbul University, 34116 Istanbul, Turkey

[28] Istanbul University Observatory Research and Application Centre, 34116 Istanbul, Turkey

[29] School of Mathematical and Physical Sciences, Macquarie University, Sydney NSW 2109, Australia

[30] Astrophysics and Space Technologies Research Centre, Macquarie University, Sydney NSW 2109, Australia

Appendix A: Additional table

Table A.1. Observation details for the 2020 October 23 occultation.

#	Site name Observer(s)	CC	Latitude (dms) Longitude (dms) Elevation (m)	Telescope (cm) Camera	Method ExpTime TimeSrc	Observation DeadTime
1	El Arenosillo *E. J. Fernández-García, A. Castro-Tirado*	ES	N 37 05 53.0 W 06 44 06.0 40	T35 Andor iXon DV-897-BV	IMG 7.0 s NTP	Positive 0.567 s
2	Granada *M. Sanchez*	ES	N 37 06 41.0 W 03 38 22.1 730	T25 ZWO ASI178M	IMG 2.0 s NTP	Positive 0.061 s
3	Sierra Nevada Observatory (OSN90) *A. Sota, PI: P. Santos-Sanz, J. Ortiz*	ES	N 37 03 46.40 W 03 23 09.35 2841	T90 Roper Scientific VersArray 2048B	IMG 3.0 s NTP	Positive 2.181 s
4	Sierra Nevada Observatory (OSN150) *A. Sota, PI: P. Santos-Sanz, J. Ortiz*	ES	N 37 03 46.52 W 03 23 09.67 2841	T150 Andor iKon-L 936 BEX2-DD	IMG 3.0 s NTP	Positive 1.848 s
5	Leeds *A. Pratt*	UK	N 53 50 15.4 W 01 36 28.0 114	T28 Watec 910HX	VID 0.64 s GPS	Negative -
6	Stevenage *S. Kidd*	UK	N 51 57 04.4 W 00 03 51.7 120	T35 ZWO ASI174 mono	IMG 0.34 s GPS	Negative -
7	Oxford *T. Haymes*	UK	N 51 55 41.2 W 01 18 46.3 199	T28 QHY174m-GPS	IMG 1.0 s GPS	Negative -
8	Abingdon *J. C. Talbot*	UK	N 51 37 53.1 W 01 16 55.2 59	T30 Watec 910HX	VID 0.64 s GPS	Negative -
9	Dourbes *R. Boninsegna*	BE	N 50 05 25.9 E 04 34 56.0 195	T40 Watec 910 HX/RC	VID 0.32 s GPS	Negative -
10	Cannet *J. J. Castellani*	FR	N 43 37 15.2 W 00 02 40.7 180	T40 Watec 120N+	VID 1.28 s GPS	Negative -
11	Istanbul University Observatory Application and Research Center (İST40) *S. Fişek, O. Çakır*	TR	N 41 00 42.48 E 28 57 56.34 60	T40 Moravian G2	IMG 0.9 s NTP	Negative -
12	Ibiza *I. de la Cueva*	ES	N 38 53 28.0 E 01 14 26.9 166	T50 SBIG STL-11000	IMG 3 s NTP	Negative 3 s
13	Albox *J. L. Maestre*	ES	N 37 24 20.0 W 02 09 06.5 493	T40 Atik 314L+	IMG 2.5 s NTP	Negative 0.8
14	Calar Alto Observatory (CAHA220) *A. Guijarro, PI: J. Ortiz, P. Santos-Sanz*	ES	N 37 13 23.30 W 02 32 46.30 2168	T220 CAFOS autoguider camera	IMG 7 s NTP	Negative 2 s
15	Las Negras *F. Casarramona*	ES	N 36 52 50.0 W 02 00 54.0 50	T20 CCD	IMG 10.0 s NTP	Negative 2.5 s
16	Teide Observatory (MUSCAT2) *E. Pallé, F. Murgas*	ES	N 28 28 28.6 W 16 18 29.0 2380	T150 CCD	IMG 20 s NTP	Negative 3 s
17	Teide Observatory (TAR1 & TAR2) *M. R. Alarcon, J. Licandro, M. Serra-Ricart*	ES	N 28 28 28.6 W 16 18 29.0 2380	T46 CCD	IMG 0.5 s NTP	Negative 0.4 ms

Notes. CC is the two-letter country code. Site latitude, longitude (format dms) and elevation (AMSL in m) are given in the WGS84 datum. Telescope: Tx is the telescope aperture in cm. Method is the recording method: IMG means digital (CDD, CMOS) sequential imaging, VID is analog video recording. TimeSrc is the used timing source and method: GPS (Global Positioning System) means 1-PPS (one pulse per second) driven video-time-insertion (VID) or camera-internal GPS timestamps (IMG). NTP denotes a Network Time Protocol computer system clock synchronization. Observation: either positive (occultation detected/recorded) or negative. ExpTime is the exposure time in seconds, DeadTime is the dead time in seconds between two subsequent images during the recording.